Bandemehr, Jascha; Baumann, Dominik; Seibald, Markus; Eklund, Kim; Karttunen, Antti J.; Kraus, Florian

Mn(IV)-Substituted Metal(II) Hexafluorido Metallates(IV): Synthesis, Crystal Structures, and Luminescence Properties

Published in:
European Journal of Inorganic Chemistry

DOI:
10.1002/ejic.202100576

Published: 07/10/2021

Document Version
Publisher's PDF, also known as Version of record

EurJIC
European Journal of Inorganic Chemistry

Full Papers
doi.org/10.1002/ejic.202100576

Chemistry Europe
European Chemical Societies Publishing

Mn(IV)-Substituted Metal(II) Hexafluorido Metallates(IV): Synthesis, Crystal Structures, and Luminescence Properties

Jascha Bandemehr,[a] Dominik Baumann,[b] Markus Seibald,[b] Kim Eklund,[c] Antti J. Karttunen,[c] and Florian Kraus*[a]

We synthesized 16 novel red-emitting Mn(IV)-substituted phosphors of the compositions $MgGeF_6$:Mn, $MgPbF_6$:Mn, Ca*M*F_6:Mn (*M*=Ge, Sn, Pb, Zr, Hf), $SrSnF_6$:Mn, "$SrTiF_6$:Mn", $BaPbF_6$:Mn, Zn*M*F_6:Mn (*M*=Sn, Pb, Zr, Hf), and Cd*M*F_6:Mn (*M*=Pb, Hf) using a dry-chemical fluorination process completely avoiding hydrofluoric acid. In comparison with the commonly used red-emitter K_2SiF_6:Mn (KSF) with its emission maximum at 630.8 nm, all above Ca and Sr compounds and $CdHfF_6$:Mn show a blue-shift of their emission maxima, the compound $SrSnF_6$:Mn even by 4.2 nm down to 626.6 nm. The compounds were characterized by powder X-ray diffraction, IR and emission spectroscopy. We additionally present the crystal structures of the unsubstituted compounds $CaZrF_6$, $CaHfF_6$, $CaPbF_6$, $CdZrF_6$, $CdHfF_6$, and $MgHfF_6$, which all crystallize isotypic in the $NaSbF_6$ structure type. The compound "$SrTiF_6$" was characterized by powder XRD and studied with evolutionary structure prediction methods, but its crystal structure could not yet be solved.

Introduction

The development and improvement of white light-emitting diodes (WLED) increased the efficiency of lighting and reduced energy consumption.[1] Such a WLED can be built exclusively out of a yellow phosphor (e.g. $Y_3Al_5O_{12}$:Ce) which is excited by blue light from a chip (e.g. $(In_xGa_{1-x})N$).[1] However, this approach greatly limits the achievable color-temperature and color-rendering index (CRI).[1] Addition of a red emitting component is required to improve such a system. Possible ones are band-emitters, like Eu(II)- or Ce(III)-substituted compounds, or line emitters where Mn(IV) is used.[2] Industrially applied are for example $Sr[LiAl_3N_4]$:Eu,[3] (Sr,Ca)$AlSiN_3$:Eu,[4] or K_2SiF_6:Mn (KSF).[5] The maximum of the red emission of K_2SiF_6:Mn is blue shifted to approximately 631 nm compared with circa 650 nm of $Sr[LiAl_3N_4]$:Eu. In general, Mn-substituted fluorides are more blue-shifted compared to oxides, for example, Mg_2GeO_4:Mn[6] shows an emission maximum at circa 660 nm.[7]

As the sensitivity of the human eye decreases with increasing wavelength,[8,9] phosphors with a comparatively short wavelength red emission (e.g. around 600 nm) are desired. Mn(IV)-substituted fluorides are the current state-of-the-art compounds with a red emission closer to the maximum light sensitivity of the human eye, and several new phosphors, such as A_2MF_6 (*A*=NH_4, Li–Cs, *M*=Si, Ge, Sn, Ti, Zr, Hf), were reported.[1,10] These compounds are typically obtained by a wet chemical process using hydrofluoric acid. Its hazardous usage can be avoided employing a mixture of H_3PO_4 and KHF_2[11] under hydrothermal conditions or a mixture of NH_4F and hydrochloric acid.[12] In both cases HF is formed in situ. Solid-state syntheses for K_3SiF_7:Mn were implemented by *Sohn* and coworkers by grinding mixtures of KHF_2, K_2SiF_6 and K_2MnF_6 under acetone, followed by drying and heating in a stream of H_2/N_2 for removal of residual HF.[13] A second solid-state route was implemented by *Jiao* and coworkers. They ground K_2TiF_6, K_2MnF_6 and KHF_2, placed the mixture in a PTFE-lined vessel, and sealed and heated it to obtain K_2TiF_6:Mn.[14] A two-step route was reported for the syntheses of K_3MOF_7:Mn (*M*=Mo, W). First, KHF_2 and MO_3 were first heated inside sealed Cu ampoules to obtain K_3MOF_7 which were then ball-milled together with K_2MnF_6 to obtain the phosphors.[15,16] A synthesis of Li_2SiF_6:Mn that avoids usage as well as formation of HF was reported. There, ground Li_2SiF_6 and Cs_2MnF_6 were heated inside a 1000 t multianvil press at a pressure of 5.5 GPa.[17] However, in all of these "HF-avoiding" syntheses the origin of K_2MnF_6 is not considered, as it is usually synthesized by a wet chemical route using HF.[18] A synthesis requiring absolutely no HF is the direct fluorination. For example, Cs_2SnF_6:Mn can be obtained from a ground mixture of CsCl, Cs_2SnCl_6 and $MnCl_2 \cdot 4H_2O$ that is heated to 350 °C in a stream of fluorine.[19] Compared with alkali metal fluorido metallates(IV), those of the alkaline earth metals are less investigated considering their potential use as red phosphors. Due to the low solubility of alkaline earth metal fluorides in water, with BaF_2 being the best soluble one, it is not unexpected that only a few barium fluorido metallates(IV) have been synthesized and substituted with Mn(IV) by wet chemical processes. These compounds are Ba[MF_6]:Mn (*M*=Si,[20] Ge,[21] Sn,[22] Ti[23]), Ba_5AlF_{13}:Mn,[24] and Ba_2ZrF_8:Mn.[25] With other

[a] J. Bandemehr, Prof. Dr. F. Kraus
Fachbereich Chemie, Philipps-Universität Marburg,
Hans-Meerwein-Str. 4, 35032 Marburg, Germany
E-mail: f.kraus@uni-marburg.de
[b] Dr. D. Baumann, Dr. M. Seibald
OSRAM Opto Semiconductors GmbH,
Mittelstetter Weg 2, 86830 Schwabmünchen, Germany
[c] K. Eklund, Prof. Dr. A. J. Karttunen
Department of Chemistry and Materials Science Aalto University, Espoo,
00076 Aalto, Finland

Supporting information for this article is available on the WWW under https://doi.org/10.1002/ejic.202100576

divalent cations, only hydrates such as $[ZnMF_6:Mn]\cdot 6H_2O$, *M*=Si,[26] Ge,[27] Sn,[28] Ti[29] were published. An easy way to synthesize AMF_6 compounds is to heat a stoichiometric mixture of starting materials such as oxides, carbonates, chlorides, fluorides or sulfates in a stream of diluted fluorine. Advantageously, the preferred oxidation state of Mn under these conditions is +IV and depending on the compound at least stable up to approximately 500 °C.[30]

We expanded the direct fluorination method of stoichiometric mixtures to synthesize homovalently Mn(IV)-substituted hexafluorido metallates(IV), employing a broad variety of potential starting materials. Under the applied fluorination conditions, we prepared compounds of the formula AMF_6, with *M* in oxidation state +IV and *A* in +II. We obtained 16 novel red phosphors for potential usage in warm white LEDs. These are $MgGeF_6$:Mn, $MgPbF_6$:Mn, $CaMF_6$:Mn (*M*=Ge, Sn, Pb, Zr, Hf), $SrSnF_6$:Mn, "$SrTiF_6$:Mn", $BaPbF_6$:Mn, $ZnMF_6$:Mn (*M*=Sn, Pb, Zr, Hf), and $CdMF_6$:Mn (*M*=Pb, Hf). We characterized the bulk compounds by powder X-ray diffraction, by IR and emission spectroscopy.

Besides these novel phosphors, we present the crystal structure of $CdZrF_6$ and propose a structure model for $CdHfF_6$. We attempted to prepare the compound of the composition "$SrTiF_6$" by various methods, obtained similar powder X-ray diffraction patterns, and can therefore report its lattice parameters for the first time.

Results and Discussion

Metal(II) hexafluorido metallates(IV) with the composition AMF_6 were prepared by direct fluorination in a stream of diluted fluorine. Heterogeneous mixtures of carbonates, chlorides, and/or oxides of *A* and *M*, as well as of $MnCl_2\cdot 4H_2O$ or a permanganate as the Mn source, were ground in agate mortars and filled into corundum boats. For details see the experimental part. The boats were placed into a heatable corundum tube through which diluted F_2 was passed. Removing the samples from the fluorine atmosphere and grinding them from time to time (on air) is important to create fresh, reactive surfaces and to avoid occlusion that could to lead to undesired side products or left over starting material, so that the samples become completely fluorinated.[31] Most of the partially and fully fluorinated samples could be handled on air for several minutes, however, after some time, depending on the compound, decomposition occurred which was observed by the appearance of a brown color. Due to this decomposition by moisture from air, all samples were transferred to an Ar-filled glove box directly after the fluorination was complete. Powder X-ray diffraction patterns were regularly taken to track the fluorination processes. The reactions were assumed to be complete when no more changes in the powder X-ray patterns were observable or when a phase pure sample had been obtained. A quick test for the successful incorporation of Mn(IV) ions into the compounds was their visually observable red luminescence using a 365 or 395 nm UV lamp as excitation source.

To analyze the obtained compounds $MgGeF_6$:Mn, $MgPbF_6$:Mn, $CaMF_6$:Mn (*M*=Ge, Sn, Pb, Zr, Hf), $SrSnF_6$:Mn, "$SrTiF_6$:Mn", $BaPbF_6$:Mn, $ZnMF_6$:Mn (*M*=Sn, Pb, Zr, Hf), and $CdMF_6$:Mn (*M*=Pb, Hf), we recorded powder X-ray diffraction patterns and carried out Le-Bail fits or Rietveld analyses, see the Supporting Information, Figures S37–S52. For the compounds $MgGeF_6$:Mn, $MgPbF_6$:Mn, $CaMF_6$:Mn (*M*=Ge, Sn, Pb, Zr, Hf), $SrSnF_6$:Mn, $BaPbF_6$:Mn, $ZnMF_6$:Mn (*M*=Sn, Pb, Zr, Hf), and $CdPbF_6$:Mn, the crystal structures are known, however, not in all cases the positions of the F atoms were reported. Table 1 shows in which structure types the compounds crystallize. Upon homovalent substitution of circa 1 to 5 at.-% of the *M*(IV) cations by Mn(IV) ions we did not observe any phase changes or polymorphism.

Table 1 shows that the structure types of $LiSbF_6$, $NaSbF_6$ are the most frequent ones, while for large *A*(II) and large *M*(IV) cations other structure types appear.

A comment on the compound with the assumed composition "$SrTiF_6$"

To the best of our knowledge, there is no proposed crystal structure model for $SrTiF_6$ in the literature. NMR spectroscopic data on "$SrTiF_6$" suggest that $[TiF_6]^{2-}$ octahedra should be present, however it is likely that accidentally $SrTiF_6\cdot 2H_2O$ instead of $SrTiF_6$ had been investigated in that report.[59]

In order to obtain "$SrTiF_6$" we reacted fluorine with heterogeneous mixtures of $SrCl_2$ and Ti powder and of $SrCl_2$ and TiS_2. In all cases similar powder X-ray diffraction patterns were obtained, all showing evidence of the same crystalline phase with some SrF_2 as a side product. Several reflections of our diffraction patterns also agree with those reported by Hagenmüller and coworkers for "$SrTiF_6$".[37] Despite many efforts we are unfortunately also not able to give a structure proposal for "$SrTiF_6$". We also cannot show conclusive evidence that a compound with the composition $SrTiF_6$ exists, yet, as a chemical

Table 1. Structure types of AMF_6 compounds presented here, where *A*=Mg, Ca, Sr, Ba, Zn, and Cd and *M*=Ge, Sn, Pb, Ti, Zr, and Hf. The given literature is the first report of the respective compound in the respective structure type. A dash means that to the best of our knowledge the crystal structure is unknown.

	Mg	Zn	Cd	Ca	Sr	Ba
Ge	$LiSbF_6$[32]	–	–	$LiSbF_6$[32]	$BaSiF_6$[32]	$BaSiF_6$[33]
Ti	$LiSbF_6$[34]	VF_3[35]	$LiSbF_6$[35]	$LiSbF_6$/$NaSbF_6$[36]	–	$BaSiF_6$[37,38]
Sn	$LiSbF_6$[39]	$LiSbF_6$[39,40]	$LiSbF_6$[40]	$NaSbF_6$/$LiSbF_6$/$CaSnF_6$[39,41]	$NaSbF_6$[39]	$BaSiF_6$/$KAsF_6$[38,39]
Zr	$NaSbF_6$/$LiSbF_6$[42–45]	$NaSbF_6$/$LiSbF_6$[42,46,47]	$NaSbF_6$	$NaSbF_6$[42,48]	$RbPaF_6$/α-$SrHfF_6$[49–51]	$RbPaF_6$/$BaZrF_6$[50–53]
Hf	–	–/$LiSbF_6$[46]	$NaSbF_6$	$NaSbF_6$[48]	$RbPaF_6$/α-$SrHfF_6$[49,52]	$RbPaF_6$[52,54]
Pb	$LiSbF_6$[55]	$LiSbF_6$[55]	VF_3[55]	$NaSbF_6$/$CaPbF_6$[56,57]	$SrPbF_6$[56–58]	$BaSiF_6$/$KAsF_6$[56,57]

analysis would only yield the composition of the bulk phase. However, in our case, bulk analysis would show if TiF_4 has been driven off during our synthesis. An elemental analysis by MP-AES confirmed a Sr:Ti ratio close to 1:1. We obtained circa 37.0(1) % for Sr, and circa 17.4(1) % for Ti, while the calculated values for $SrTiF_6$ are 35.0 % Sr and 18.2 % Ti. As the "$SrTiF_6$" had to be dissolved and diluted to obtain a solution with a concentration suitable for MP-AES, an additional error is certainly introduced which is not included in the above numbers. The analysis shows however, that only little TiF_4 was lost, if at all. We therefore assume that the composition of the sample is $SrTiF_6$ or very close to it.

Our powder X-ray diffraction patterns are shown in Figure S42, Figure S57 and Figure S58. We could index the powder patterns with two related tetragonal unit cells, the first one with lattice parameters $a = 9.669(1)$, $c = 9.4299(13)$ Å, $V = 881.60(18)$ Å^3, and the second one with $a' = \sqrt{2} \cdot a = 13.674$ Å, c, $V = 1764$ Å^3. We calculated the volume of a $SrTiF_6$-unit by adding the volumes of SrF_2- and TiF_4-units, obtained from their respective crystal structures, to circa 118 Å^3. For the lattice parameters given above this would lead to a Z of 7.5 and 14.9, respectively. For comparison, Table 2 lists lattice parameters, space groups and Pearson symbols of putatively related compounds of the composition AMF_6 (A=Ca–Ba, M=Ti, Rh).

$CaTiF_6$ has been described in two different modifications, crystallizing in the $LiSbF_6$ and $NaSbF_6$ structure types, respectively. When the A(II) cation increases in size, the $BaSiF_6$ structure type is observed. We included $SrRhF_6$ in Table 2 due to the similar ionic radii of Rh(IV) and Ti(IV) in octahedral coordination.[61] We note that $SrRhF_6$ and $BaTiF_6$ both crystallize in the $BaSiF_6$ structure type, so it is peculiar as to why $SrTiF_6$ doesn't. Hagenmüller and coworkers reported that $SrTiF_6$ might crystallize in the monoclinic crystal system.[37] In the IR spectrum of "$SrTiF_6$" (also see below) we observe six bands which indicates lower site symmetry for the $[TiF_6]^{2-}$ anions. All our attempts to grow single crystals of $SrTiF_6$ suitable for the diffraction experiment were so far unsuccessful and we are therefore currently unable to give a definite answer.

We carried out searches for potential crystal structures of "$SrTiF_6$" using quantum chemical methods and the USPEX evolutionary algorithm. The full computational methodology is described in the experimental section. Over 1500 structures were investigated using the composition with 2 to 8 formula units in the primitive cell. The evolutionary algorithm gave the cubic $CaTiF_6$ crystal structure ($NaSbF_6$ structure type) as the lowest-energy structure for $SrTiF_6$ ($Fm\bar{3}m$, $V = 640$ Å^3, $Z = 4$). However, an orthorhombic crystal structure in space group $Iba2$ ($V = 908$ Å^3, $Z = 8$) was only 2.7 kJ/mol per formula unit higher in energy. The volume of the calculated unit cell is rather close to the 881.6 Å^3 for the tetragonal unit cell obtained from powder X-ray diffraction. The lattice parameters of the hypothetical orthorhombic structure are $a = 9.83$, $b = 9.60$, and $c = 9.63$ Å. Attempts to perform a Le Bail fit with these values, did not show convergence and the lattice parameters were refined to be similar to those indexed on the powder X-ray diffraction pattern. Finally, a trigonal structure ($R3$, $V = 1368$ Å^3, $Z = 12$, i.e. 4 formula units in the primitive cell) also showed a relatively low energy difference of 5.3 kJ/mol per formula unit compared to the cubic $CaTiF_6$-type structure. The USPEX structural searches up to 8 formula units in primitive cell failed to produce any low-energy structures and resulted in low-symmetry structures, in line with our previous experiences with the same structure prediction methodology.[62,63] Therefore, we did not investigate any compositions with more than 8 formula units in the primitive cell. The optimized structures of the lowest-energy structural candidates, together with their simulated powder X-ray diffraction patterns, are provided in the Supporting Information in CIF format.

The crystal structures of $CaMF_6$ (M = Zr, Hf, Pb)

$CaZrF_6$,[42,48] $CaHfF_6$,[48] and $CaPbF_6$[56,57] crystallize in the $NaSbF_6$ structure type in space group $Fm\bar{3}m$ (no. 225, $cF32$), where of all atom positions solely the x coordinate of the F atom is refinable and has not been reported, respectively. We performed powder X-ray diffraction measurements on these compounds and carried out Rietveld refinements. Their details are listed in Table S20, Table S22 and Table S24 and the powder X-ray diffraction patterns are shown in Figures S53–S55. The refined lattice parameters are $a = 8.47463(17)$ Å, $V = 608.64(2)$ Å^3 for $CaZrF_6$, $a = 8.4598(2)$ Å, $V = 605.46(3)$ Å^3 for $CaHfF_6$, and $a = 8.4924(2)$ Å, $V = 612.48(2)$ Å^3 for $CaPbF_6$, all with $Z = 4$ and $T = 293$ K in space group $Fm\bar{3}m$ (no. 225, $cF32$). The x coordinate of the F atoms is 0.237(2) for $CaZrF_6$, 0.238(2) for $CaHfF_6$, and 0.239(2) for $CaPbF_6$. These values agree considering the standard uncertainties, which is plausible due to the similar atomic radii of Zr(IV), Hf(IV) and Pb(IV).[61] Therefore, the M–F bond lengths are also quite similar with 2.007(13) Å for M=Zr, 2.016(13) Å for M=Hf, and 2.026(18) Å for M=Pb. They agree with reported ones of 2.04 Å in $BaMF_6$ (M=Zr,[51] Hf,[54] Pb[57]).

Table 2. A comparison of lattice parameters, space groups and Pearson symbols of $ATiF_6$ compounds (A=Ca–Ba, M=Ti, Rh). $SrRhF_6$ has been included due to the similar ionic radii of Ti(IV) and Rh(IV) in octahedral coordination.

	a	c	V	Z	Space group	Pearson symbol	Structure type
$CaTiF_6$[36]	5.66	14.2	395	3	$R\bar{3}$	$hR24$	$LiSbF_6$
$CaTiF_6$[36]	8.16	a	542	4	$Fm\bar{3}m$	$cF32$	$NaSbF_6$
$SrRhF_6$[60]	7.15	6.95	308	3	$R\bar{3}m$	$hR24$	$BaSiF_6$
"$SrTiF_6$"	9.669(1)	9.4299(13)	881.60(18)	7.5			
"$SrTiF_6$"	$13.674 = \sqrt{2} \cdot 9.669$	9.44	1764	14.9			
$BaTiF_6$[38]	7.37	7.25	341	3	$R\bar{3}m$	$hR24$	$BaSiF_6$

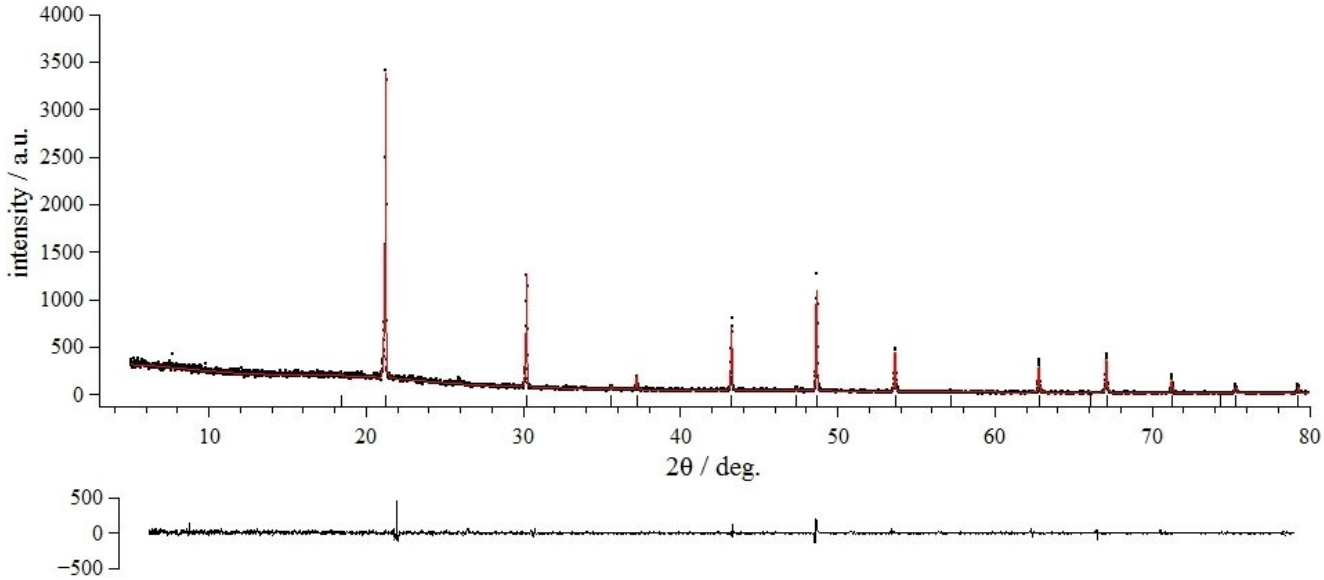

Figure 1. Observed (black) and calculated (red) powder X-ray pattern of $CdZrF_6$ after Rietveld refinement. The calculated reflection positions are indicated by the vertical bars below the patterns. The curve at the bottom represents the difference between the observed and the calculated intensities. $R_p = 8.33$, $R_{wp} = 11.12$ (not background corrected), $S = 1.13$.

Atom positions and isotropic displacement parameters are listed in Table S21, Table S23 and Table S25.

The crystal structures of $CdMF_6$ (M = Zr, Hf)

To the best of our knowledge, neither lattice parameters nor structure proposals have been reported for $CdZrF_6$ and $CdHfF_6$. According to our Rietveld refinement (Figure 1) on the powder X-ray diffraction pattern of $CdZrF_6$ it crystallizes in the $NaSbF_6$ structure type in space group $Fm\bar{3}m$, with $a = 8.3684(2)$ Å, $V = 586.05(2)$ Å^3, $Z = 4$, $T = 293$ K. Refinement details are listed in Table 3, atom positions and isotropic displacement parameters are listed in Table 4. We refined all atoms with isotropic displacement parameters. The Zr–F bond length is with 2.00(3) Å comparable to others within octahedral $[ZrF_6]^{2-}$ anions, for example 2.04 Å in Rb_2ZrF_6.[64]

Attempts to substitute some Zr(IV) by Mn(IV) cations did not lead to the compound $CdZrF_6$:Mn, yet. Surprisingly however, we obtained a red-emitting phosphor containing some Mn(IV) ions in the case of $CdHfF_6$. The lattice parameters of $CdHfF_6$:Mn are with $a = 8.348(2)$ Å, $V = 581.8(1)$ Å^3, $T = 293$ K similar to those of $CdZrF_6$, which is why we can safely assume that $CdHfF_6$:Mn crystallizes isotypic to $CdZrF_6$ in the $NaSbF_6$ structure type. We therefore assume that the unsubstituted compound $CdHfF_6$ is also isotypic. For $CdHfF_6$:Mn we do not report the Hf–F bond length here as it would be biased due to the presence of the Mn(IV) atoms.

Table 3. Selected crystallographic data and details of the structure determination of $CdZrF_6$.

Formula	$CdZrF_6$
Molar mass/g·mol^{-1}	317.6
Space group (No.)	$Fm\bar{3}m$ (225)
a/Å	8.36844(18)
V/Å^3	586.05(2)
Z	4
Pearson symbol	$cF32$
ρ_{calc}/g·cm^{-3}	3.5998
Color of the powder	colorless
T/K	293
λ/Å	1.54060 (Cu–Kα_1)
$2\theta_{min}$, $2\theta_{max}$, $2\theta_{step}$/°	5.000, 81.08, 0.015
No. of data points	5073
No. of parameters	11
No. of restraints	0
No. of constraints	0
Peak shape function	Pseudo-Voigt
Background	manual
S	1.13
R_P, R_{wp} [a]	8.33, 11.12
$R_B(I)$	3.86
$\Delta\rho_{max}$, $\Delta\rho_{min}$/e·Å^{-3}	0.30, −1.16

[a] Not background-corrected R-factors

Table 4. Atomic coordinates and equivalent isotropic displacement parameters U_{iso} for $CdZrF_6$.

Atom	Position	x	y	z	U_{iso}/Å^2
Cd	4*b*	1/2	1/2	1/2	0.017(3)
Zr	4*a*	0	0	0	0.023 (3)
F	24*e*	0.239(4)	0	0	0.046(5)

The crystal structure of $MgHfF_6$

To the best of our knowledge no crystal structure has been reported so far for $MgHfF_6$. However, the certainly closely related compound $MgZrF_6$ is known to be dimorphic and crystallizes both in the $NaSbF_6$ and $LiSbF_6$ structure types.[42–45] We performed powder X-ray diffraction analysis on a sample which contained $MgHfF_6$, HfF_4, and MgF_2. According to the Rietveld refinement (Figure S56), $MgHfF_6$ crystallizes in the $NaSbF_6$ structure type with the lattice parameter $a = 7.9183(2)$ Å, $V = 496.46(2)$ Å^3 with $Z = 4$ at $T = 293$ K in space group $Fm\bar{3}m$ (no. 225, *cF*32). The *x* coordinate of the F atom was refined to 0.2546(13) which resulted in a Hf–F bond length of 2.016(10) Å. This value agrees with 2.04 Å in $BaHfF_6$.[54] Refinement details and isotropic displacement parameters are given in Table S26 and Table S27.

Infrared spectroscopic investigation of the presented compounds

In pure hexafluorido manganates(IV) as well as in compounds where some *M*(IV) ions have been substituted with Mn(IV), the Mn–F stretching vibrations (F_{1u}) of the $[MnF_6]^{2-}$ anions are usually observed around 620 cm^{-1}.[65,66] Due to the small amount (≈1–5 at.-%) of Mn(IV) ions, the vibration could not be observed in most of the recorded spectra and it may have been sometimes obscured by the much more intense *M*–F vibration. However, we were able to observe the Mn–F stretch in the compound $CaPbF_6$:Mn where the Mn-content is circa 5 %. Its IR spectrum is shown in Figure 2 and compared with unsubstituted $CaPbF_6$ in Figure S59.

The IR spectra of the other compounds are shown in Figures S60–S77. Nearly all of the spectra show only one band, which arises from the stretching vibration (F_{1u}) of the octahedron-like or octahedral, depending on site symmetry, $[MF_6]^{2-}$ anion.[67] Only "$SrTiF_6$" shows six vibrations in this region, which is why we assume a lower site symmetry for the probably octahedron-like $[TiF_6]^{2-}$ anion in comparison with those compounds crystallizing in trigonal or cubic crystal systems. In all samples, no additional bands are visible in the recorded region between 4000 and 400 cm^{-1}. This indicates that essentially no hydrolysis products or other OH containing impurities are present.

The luminescence of AMF_6:Mn compounds

All of the above mentioned Mn-substituted compounds exhibit a red-light emission when irradiated with UV light of suitable wavelength. The excitation spectrum for $CaZrF_6$:Mn is shown in Figure 3 and the emission spectrum, compared with K_2SiF_6:Mn is shown in Figure 4. All other luminescence spectra are shown in Figures S22–S36.

Seven emission lines arise from K_2SiF_6:Mn. They correspond to the parity and spin-forbidden $^2E_g \rightarrow {}^4A_{2g}$ transition, observed at approximately 598, 609, 612, 620, 631, 635, and 648 nm (dashed curve in Figure 4).[5,10] From left to right, they can be assigned to the $\nu_3(t_{1u})$, $\nu_4(t_{1u})$, and $\nu_6(t_{2u})$ vibrations, to the zero-phonon-line (ZPL), and to the $\nu_6(t_{2u})$, $\nu_4(t_{1u})$ and $\nu_3(t_{1u})$ vibrations, respectively. Due to the high symmetry of the coordination polyhedron around the Mn(IV) cation in K_2SiF_6:Mn the intensity of the ZPL is too low to be observed.[68] In $CaZrF_6$:Mn more emission lines are recorded in comparison with K_2SiF_6:Mn and even the ZPL could be detected with low intensity. The maximum of the emission line was observed at 628.3 nm, which is blue-shifted compared to the maximum of 630.8 nm in K_2SiF_6:Mn.

The most hypsochromic shift of the emission lines among the AMF_6:Mn compounds presented here was observed for $SrSnF_6$:Mn, with an emission maximum at 626.6 nm. As mentioned above, the sensitivity of the human eye decreases

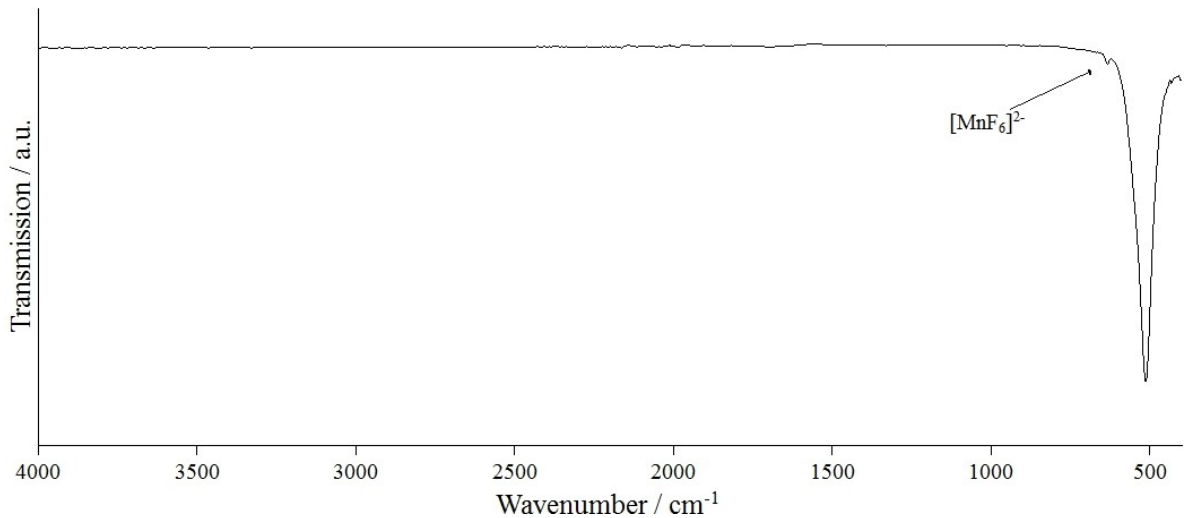

Figure 2. ATR-IR spectrum of $CaPbF_6$:Mn. The Mn–F stretching vibration (F_{1u}) of $[MnF_6]^{2-}$ can be observed as a weak band at 638 cm^{-1}, whereas the Pb–F stretching vibration (F_{1u}) of $[PbF_6]^{2-}$ is observed at 512 cm^{-1}.

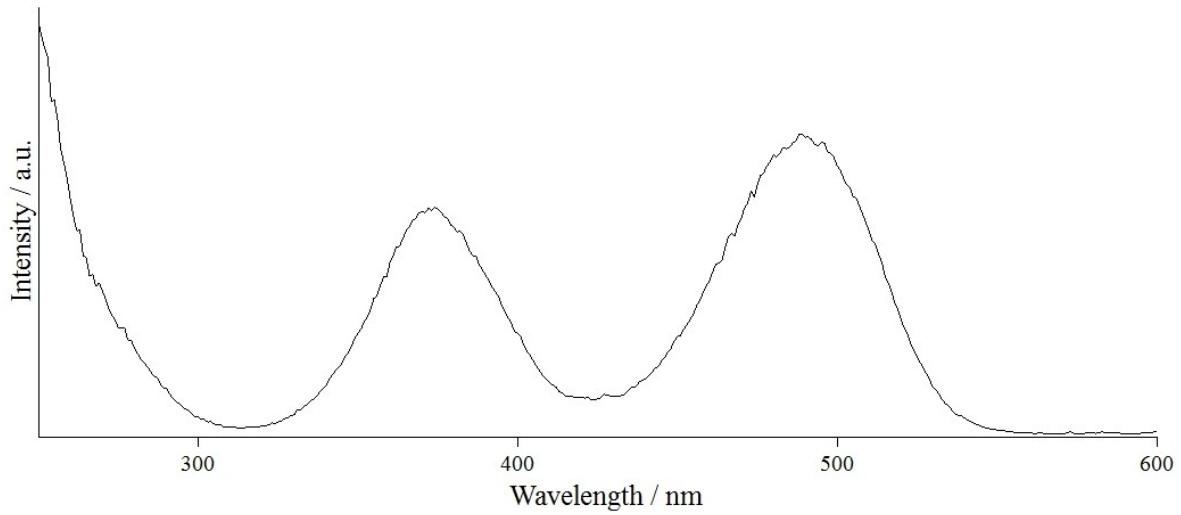

Figure 3. Excitation spectrum of $CaZrF_6$:Mn monitored at 628 nm. The two emissions bands can be assigned to the $^4A_{2g}\rightarrow{}^4T_{1g}$ (left) and $^4A_{2g}\rightarrow{}^4T_{2g}$ (right).[10]

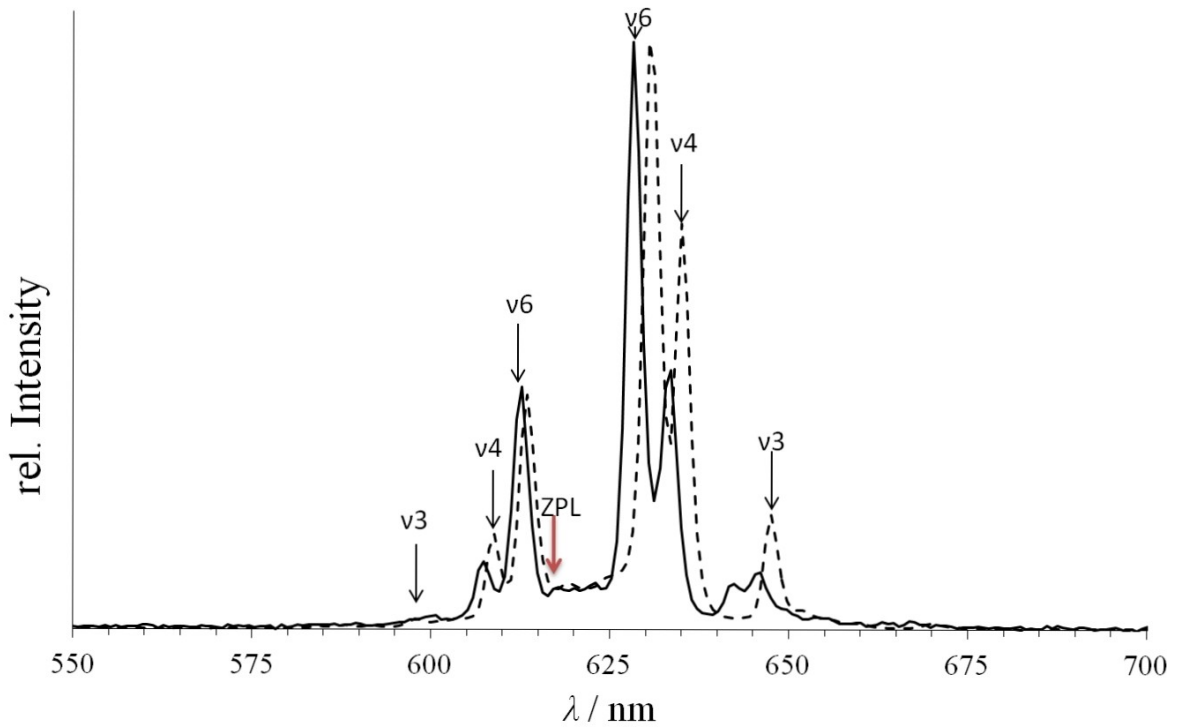

Figure 4. Emission spectrum of $CaZrF_6$:Mn (continuous black line) excited at 490 nm, compared with K_2SiF_6:Mn (dashed line). The arrows indicate the maxima of the band positions for K_2SiF_6:Mn, the position of its unobserved zero-phonon-line is indicated with the red arrow.

with increasing wavelength, which is why even small blue-shifts with respect to K_2SiF_6:Mn result in significant increases of the value of the luminous efficacy of the radiation (LER). The perceived colors are described by the CIE coordinates and the dominant wavelength λ_{dom} (wavelength of monochromatic light that elicits the same perception of hue as the described spectrum), and they are listed beside the maximum of luminescence and the LER value for all above mentioned compounds in Table 5.

We note that all Zn compounds of the composition AMF_6:Mn ($M = Zr$, Hf, Sn, Pb) show a bathochromic shift, while all Ca and Sr compounds are blue-shifted compared with K_2SiF_6:Mn. All Ba compounds show similar ($BaSiF_6$:Mn) or red-shifted emission maxima. Seemingly, from the compounds presented here, the emission of Mn-substituted compounds crystalizing in the cubic $NaSbF_6$ structure type is shifted hypsochromic, while those belonging to the $LiSbF_6$ structure type are red-shifted. In other words, those compounds with

Table 5. Comparison of the emission maximum λ_{max}, the dominant wavelength λ_{dom}, the *x* and *y* coordinate of the CIE 1931 color space, and the LER (luminous efficacy of radiation) value of the synthesized AMF_6:Mn compounds and of K_2SiF_6:Mn, Ba*M*'F_6:Mn (*M*'=Si, Ge, Sn, Ti) for comparison. The site symmetry is given for the position of the *M*(IV) atoms as Hermann-Mauguin and Schoenflies symbols. The standard uncertainty of the wavelengths and CIE coordinates is circa 2 for the last digit.

Formula	λ_{max}	λ_{dom}	*CIE-x*	*CIE-y*	LER/lm W_{opt}^{-1}	Structure type	Site symmetry
$SrSnF_6$:Mn	626.6	617.2	0.685	0.314	228.6	$NaSbF_6$	$m\bar{3}m$ (O_h)
$CdHfF_6$:Mn	627.3	609.9	0.665	0.334	[a]	$NaSbF_6$	$m\bar{3}m$ (O_h)
$CaZrF_6$:Mn	628.3	615.4	0.681	0.319	222.2	$NaSbF_6$	$m\bar{3}m$ (O_h)
$CaHfF_6$:Mn	628.3	617.2	0.685	0.315	219.3	$NaSbF_6$	$m\bar{3}m$ (O_h)
$CaSnF_6$:Mn	628.5	609.0	0.663	0.337	229.9	$NaSbF_6$	$m\bar{3}m$ (O_h)
"$SrTiF_6$:Mn"	628.4	612.7	0.674	0.326	190.7	?	
$CaGeF_6$:Mn	628.6	597.7	0.616	0.383	[a]	$LiSbF_6$	$\bar{3}$. (S_6)
$CaPbF_6$:Mn	629.1	618.6	0.689	0.311	213.4	$NaSbF_6$	$m\bar{3}m$ (O_h)
$BaSiF_6$:Mn[69]	630					$BaSiF_6$	$\bar{3}m$ (D_{3d})
K_2SiF_6:Mn	630.8	619.6	0.689	0.311	204,9	K_2PtCl_6	$m\bar{3}m$ (O_h)
$CdPbF_6$:Mn	631.5	615.7	0.682	0.318	206.8	VF_3	$\bar{3}$. (S_6)
$MgGeF_6$:Mn	632.0	614.5	0.679	0.321	185.6	$LiSbF_6$	$\bar{3}$. (S_6)
$BaSnF_6$:Mn[22]	632					$KAsF_6$	$\bar{3}$. (S_6)
$BaPbF_6$:Mn	632.5	620.6	0.693	0.307	191.4	$BaSiF_6$	$\bar{3}m$ (D_{3d})
$ZnSnF_6$:Mn	632.6	615.5	0.681	0.318	202.3	$LiSbF_6$	$\bar{3}$. (S_6)
$ZnHfF_6$:Mn	632.7	617.7	0.687	0.313	194.9	$LiSbF_6$	$\bar{3}$. (S_6)
$ZnPbF_6$:Mn	632.8	616.6	0.684	0.316	181.0	$LiSbF_6$	$\bar{3}$. (S_6)
$ZnZrF_6$:Mn	632.8	616.5	0.684	0.316	195.1	$NaSbF_6$	$m\bar{3}m$ (O_h)
$MgPbF_6$:Mn	633.0	613.3	0.675	0.324	205.2	$LiSbF_6$	$\bar{3}$. (S_6)
$BaTiF_6$:Mn[23]	633					$BaSiF_6$	$\bar{3}m$ (D_{3d})
$BaGeF_6$:Mn[70]	634		0.695	0.305		$BaSiF_6$	$\bar{3}m$ (D_{3d})

[a] No data are given due to a bad signal to noise ratio.

Mn(IV) atoms on sites of $m\bar{3}m$ (O_h) symmetry seem to lead to the most blue-shifted emissions, with the exception of the Zn compound $ZnZrF_6$:Mn. Despite quite similar ways of syntheses, we obtained the compounds $ZnZrF_6$:Mn and $ZnHfF_6$:Mn in different structure types. Unsubstituted $ZnZrF_6$ is known to be dimorphic,[42,46,47] so it is extremely likely that $ZnHfF_6$ is also dimorphic. The difference of the location of the emission maximum of $ZnHfF_6$:Mn and $CdHfF_6$:Mn may be due to the different structure types we obtained the compounds in or due to the differences in the chemical hardness of Zn^{2+} and Cd^{2+}. Further investigations are needed to obtain compounds as well as other polymorphs.

The quantum efficiencies of the prepared samples were between 1 and 51%. The syntheses were not optimized to improve the quantum efficiencies as these values are also influenced by decomposition of the air sensitive compounds during the preparation and measurement. Due to the decomposition of the samples on air, we only measured the thermal quenching of $CaZrF_6$:Mn (Figure S80), which already starts at lower temperatures compared to KSF.[71]

Conclusion

The novel red-emitting Mn(IV)-substituted phosphors $MgGeF_6$:Mn, $MgPbF_6$:Mn, Ca*M*F_6:Mn (*M*=Ge, Sn, Pb, Zr, Hf), $SrSnF_6$:Mn, "$SrTiF_6$:Mn", $BaPbF_6$:Mn, Zn*M*F_6:Mn (*M*=Sn, Pb, Zr, Hf), and Cd*M*F_6:Mn (*M*=Pb, Hf) have been obtained by direct fluorination. The syntheses of most of these Mn-substituted ternary fluorides via the common route using hydrofluoric acid solutions is difficult or impossible, as some of the binary fluorides have very low solubility or are redox-unstable in acidic aqueous medium such as Pb(IV). The compounds crystallize in various structure types and no relation to the emission wavelength was recognized. Crystal structure predictions for the composition "$SrTiF_6$" yielded the $CaTiF_6$ ($NaSbF_6$) structure as the lowest-energy structural candidate, but an orthorhombic crystal structure (*Iba*2) was only 2.5 kJ/mol per formula unit higher in energy. Neither structure matched perfectly with the recorded powder X-ray diffraction pattern and the crystal structure of "$SrTiF_6$" remains unsolved so far. Seemingly, the phosphors crystallizing in the cubic $NaSbF_6$ structure type show the most blue-shifted emission maxima, with $SrSnF_6$:Mn at 626.6 nm. The latter emission is by 4.2 nm blue-shifted in comparison with the one from the commonly used K_2SiF_6:Mn (KSF).

Experimental Section

Caution! F_2 is a rather powerful oxidant and may pose a working hazard to those being unexperienced, untrained, and unskilled and therefore proper safety measures and emergency treatment need to be available.

Syntheses of metal(II) hexafluorido metallates(IV): All compounds of the general composition AMF_6 were synthesized by direct fluorination of stoichiometric mixtures of salts containing the *A*(II) and salts containing the *M*(IV) ions. Used salts are listed in Table S1. The heterogeneous mixtures were ground in agate mortars and loaded into corundum boats. The boats were placed into heatable corundum tubes through which 10% fluorine in argon (V/V) was

passed. The reaction mixtures were slowly heated up to the respective temperature upon which fluorination was complete. To obtain Mn(IV)-substituted compounds, circa 1 to 5 at.-% of the *M*(IV) salt was replaced by $MnCl_2 \cdot 4H_2O$ or another Mn containing compound (see Table S1). For complete fluorination, the samples had to be taken out of the oven and ground regularly using a glassy carbon mortar. Then, the samples were fluorinated again. The process of grinding and fluorination was repeated until no more changes in the powder X-ray diffraction patterns occurred or a phase pure sample had been obtained. Due to the presence of MgF_2 in the powder X-ray pattern of $MgGeF_6$:Mn and the identical ionic radii of Ge(IV) and Mn(IV), we performed an elemental analysis on this sample to determine if gaseous GeF_4 and MnF_4 were lost during synthesis. The result of this elemental analysis is 33.7(1) wt.-% Mg, 3.44(1) wt.-% Ge and 0.25 wt.-% Mn, which indicates, combined with the information gained from the powder X-ray pattern, that a compound containing both manganese and germanium, should be present and we assume its composition as $MgGeF_6$:Mn.

Powder X-ray diffraction: The powder X-ray diffraction patterns were recorded at ambient temperature with a STOE Stadi MP powder diffractometer in modified Debye-Scherrer geometry (capillary) or transmission geometry (flat sample). The diffractometer was operated with Cu–Kα_1 radiation (1.5406 Å, Ge(111) monochromator) and equipped with a Mythen1 K detector. The samples, which were measured in modified Debye-Scherrer geometry, were sealed under inert gas atmosphere (argon 5.0, Praxair) in a glass capillary (WJM Glas). The samples in transmission geometry were measured between two pieces of a Scotch tape (3MScotch® Magic™). The evaluation of the powder X-ray patterns were carried out with the WinXPOW 3.07 software package.[72] The Rietveld refinements and Le-Bail fits were performed with Jana2006.[73]

IR spectroscopy: Infrared spectra were measured on a Bruker Alpha Platinum FT-IR spectrometer using the ATR Diamond module with a resolution of 4 cm^{-1}. The spectrometer was located inside a glovebox under argon (5.0, Praxair) atmosphere. For data collection, the OPUS 7.2 software was used.[74]

Elemental Analysis: Samples for elemental analyses were dissolved in Millipore H_2O (Synergy R UV-R) and a small amount of nitric acid (65 %, VWR, AnalaR NORMAPUR). Analyses were carried out via microwave plasma-atomic emission spectroscopy (4200 MP-AES, Agilent).

Luminescence spectroscopy: The luminescence spectra, monitored at 488 nm, were recorded using a solid-state laser with a Monovista CRS+ confocal Raman microscope (Spectroscopy & Imaging GmbH). The other spectra and quantum efficiency (QE) were measured using a QUANTAURUS-QY spectrometer (HAMAMATSU, Japan) equipped with a full integrating sphere (diameter approx. 8.4 cm) and a 150 W xenon excitation light source. In order to prevent fluorescence of the sample container, the sample was measured inside a closed silica-glass cell (outer diameter 17 mm) positioned on a PTFE covered sample holder. The excitation wavelength with a maximum spectral full width at half maximum (FWHM) of 10 nm was chosen according to the sample. A spectrum was measured in the wavelength range between 550 nm and 700 nm with 0.77 nm step size.

Computational details: Version 9.4.4 of the USPEX code was used for the crystal structure predictions of "$SrTiF_6$".[75–77] Quantum chemical calculations within the USPEX simulations were carried out with the CRYSTAL[78] code using the USPEX interface we have developed.[79] In the DFT calculations, we applied a hybrid PBE0 functional with 25 % Hartree-Fock exchange.[80,81] In the USPEX simulations, we applied Gaussian-type split-valence + polarization (SVP) derived from molecular Karlsruhe def2 basis sets (see Supporting information for basis set details.[82]

In the USPEX simulations, we used different numbers of formula units in the primitive cell to study the configuration space of the unknown crystal structure of "$SrTiF_6$". Crystal structures were investigated for the composition with 2, 3, 4, and 8 formula units in the primitive cell. For each crystal structure, two USPEX runs were performed. To speed up the evolutionary searches, the CRYSTAL geometry optimizations within the USPEX simulations were carried out with looser convergence criteria compared to the criteria reported below. Three structural optimizations with increasingly strict convergence criteria were carried out for each structural candidate. A reciprocal space *k*-point density of 0.14, 0.12, and 0.10 2π Å^{-1} was applied for the first, second, and third optimization steps, respectively. Input examples for USPEX and CRYSTAL are included in the Supporting Information.

The lowest-energy structures from each USPEX simulation were re-optimized at the DFT-PBE0/TZVP level of theory (SVP basis set for Sr) and the default CRYSTAL convergence criteria. Reciprocal space *k*-point meshes were chosen in such way that the reported energies are converged to about 0.1 kJ/mol per atom. Tightened tolerance factors (TOLINTEG) of 8, 8, 8, 8 and 16 were used for the evaluation of the Coulomb and exchange integrals. The low-energy "$SrTiF_6$" structures discussed here were confirmed as true local minima by means of harmonic frequency calculations.[83,84]

Acknowledgements

We thank the X-ray facilities at the Philipps-Universität Marburg for their services. Furthermore, we thank M. Möbs and B. Koch, Philipps-Universität Marburg, for recording Raman spectra. A. J. K. thanks CSC – the Finnish IT Center for Science for computing resources. We thank Anja Köbler for support with the photoluminescence measurements. Open Access funding enabled and organized by Projekt DEAL.

Conflict of Interest

The authors declare no conflict of interest.

Keywords: Fluorides · Luminescence · Phosphors · Quantum-chemical calculations · Structure elucidation

[1] Q. Zhou, L. Dolgov, A. M. Srivastava, L. Zhou, Z. Wang, J. Shi, M. D. Dramićanin, M. G. Brik, M. Wu, *J. Mater. Chem. C* **2018**, *6*, 2652–2671.
[2] J. W. Moon, B. G. Min, J. S. Kim, M. S. Jang, K. M. Ok, K.-Y. Han, J. S. Yoo, *Opt. Mater. Express* **2016**, *6*, 782.
[3] P. Pust, V. Weiler, C. Hecht, A. Tücks, A. S. Wochnik, A.-K. Henß, D. Wiechert, C. Scheu, P. J. Schmidt, W. Schnick, *Nat. Mater.* **2014**, *13*, 891–896.
[4] H. Watanabe, N. Kijima, *J. Alloys Compd.* **2009**, *475*, 434–439.
[5] S. Adachi, T. Takahashi, *J. Appl. Phys.* **2008**, *104*, 023512.
[6] S. Kawakita, H. Kominami, K. Hara, *Phys. Status Solidi C* **2015**, *12*, 805–808.
[7] D. Chen, Y. Zhou, J. Zhong, *RSC Adv.* **2016**, *6*, 86285–86296.
[8] A. Stockman, L. T. Sharpe, *Vision Res.* **2000**, *40*, 1711–1737.
[9] CIE, *Fundamental Chromaticity Diagram with Physiological Axes. Parts 1 and 2. Technical Report 170–1*, Central Bureau Of The Commission Internationale De L' Éclairage, Wien, **2006**.

[10] S. Adachi, *ECS J. Solid State Sci. Technol.* **2020**, *9*, 016001.
[11] L. Huang, Y. Zhu, X. Zhang, R. Zou, F. Pan, J. Wang, M. Wu, *Chem. Mater.* **2016**, *28*, 1495–1502.
[12] Z. Hou, X. Tang, X. Luo, T. Zhou, L. Zhang, R.-J. Xie, *J. Mater. Chem. C* **2018**, *6*, 2741–2746.
[13] M. Kim, W. B. Park, B. Bang, C. H. Kim, K.-S. Sohn, *J. Am. Ceram. Soc.* **2017**, *100*, 1044–1050.
[14] S. Zhang, H. Wei, Y. Zhou, X. Wang, L. Xu, H. Jiao, *Opt. Mater.* **2018**, *86*, 165–171.
[15] C. Stoll, M. Seibald, D. Baumann, H. Huppertz, *Eur. J. Inorg. Chem.* **2019**, *2019*, 3383–3388.
[16] C. Stoll, G. Heymann, M. Seibald, D. Baumann, H. Huppertz, *J. Fluorine Chem.* **2019**, *226*, 109356.
[17] C. Stoll, J. Bandemehr, F. Kraus, M. Seibald, D. Baumann, M. J. Schmidberger, H. Huppertz, *Inorg. Chem.* **2019**, *58*, 5518–5523.
[18] R. F. Weinland, O. Lauenstein, *Z. Anorg. Allg. Chem.* **1899**, *20*, 40–45.
[19] A. G. Paulusz, *J. Lumin.* **1978**, *17*, 375–384.
[20] D. Sekiguchi, J. Nara, S. Adachi, *J. Appl. Phys.* **2013**, *113*, 183516.
[21] D. Sekiguchi, S. Adachi, *Opt. Mater.* **2015**, *42*, 417–422.
[22] R. Hoshino, T. Nakamura, S. Adachi, *ECS J. Solid State Sci. Technol.* **2016**, *5*, R37–R43.
[23] D. Sekiguchi, S. Adachi, *ECS J. Solid State Sci. Technol.* **2014**, *3*, R60–R64.
[24] L. Qin, P. Cai, C. Chen, J. Wang, H. J. Seo, *RSC Adv.* **2017**, *7*, 49473–49479.
[25] M. Gu, Y. Tian, C. Cui, P. Huang, L. Wang, Q. Shi, *Mater. Res. Bull.* **2018**, *107*, 242–247.
[26] R. Hoshino, S. Adachi, *J. Appl. Phys.* **2013**, *114*, 213502.
[27] R. Hoshino, S. Adachi, *J. Lumin.* **2015**, *162*, 63–71.
[28] R. Hoshino, S. Adachi, *Opt. Mater.* **2015**, *48*, 36–43.
[29] R. Hoshino, S. Sakurai, T. Nakamura, S. Adachi, *J. Lumin.* **2017**, *184*, 160–168.
[30] E. Huss, W. Klemm, *Z. Anorg. Chem.* **1950**, *262*, 25–32.
[31] R. Hoppe, B. Hofmann, *Z. Anorg. Allg. Chem.* **1977**, *436*, 65–74.
[32] D. Reinen, F. Steffens, *Z. Anorg. Allg. Chem.* **1978**, *441*, 63–82.
[33] J. L. Hoard, W. B. Vincent, *J. Am. Chem. Soc.* **1940**, *62*, 3126–3129.
[34] K. Persson, Materials Data on MgTiF6 (SG:148) by Materials Project, **2014**, Web. doi:10.17188/1319275.
[35] R.-H. Odenthal, R. Hoppe, *Z. Anorg. Allg. Chem.* **1971**, *384*, 104–110.
[36] B. R. Hester, A. P. Wilkinson, *Inorg. Chem.* **2018**, *57*, 11275–11281.
[37] J. Ravez, M. Vassiliadis, R. Von der Mühll, P. Hagenmüller, *Rev. Chim. Miner.* **1970**, 967–973.
[38] S. Becker, G. Benner, R. Hoppe, *Z. Anorg. Allg. Chem.* **1990**, *591*, 7–16.
[39] P. J. Moehs, H. M. Haendler, *Inorg. Chem.* **1968**, *7*, 2115–2118.
[40] R. Hoppe, V. Wilhelm, B. Müller, *Z. Anorg. Allg. Chem.* **1972**, *392*, 1–9.
[41] H. W. Mayer, D. Reinen, G. Heger, *J. Solid State Chem.* **1983**, *50*, 213–224.
[42] M. Poulain, J. Lucas, *C. R. Seances Acad. Sci. Ser. C* **1970**, 822–824.
[43] B. R. Hester, J. C. Hancock, S. H. Lapidus, A. P. Wilkinson, *Chem. Mater.* **2017**, *29*, 823–831.
[44] J. Xu, L. Hu, Y. Song, F. Han, Y. Qiao, J. Deng, J. Chen, X. Xing, *J. Am. Ceram. Soc.* **2017**, *100*, 5385–5388.
[45] A. V. Gerasimenko, K. A. Gaivoronskaya, A. B. Slobodyuk, N. A. Didenko, *Z. Anorg. Allg. Chem.* **2017**, *643*, 1785–1792.
[46] R. L. Davidovich, T. F. Levchishina, S. B. Ivanov, *Inorg. Mater.* **1975**, *11*, 1872–1875.
[47] V. Rodriguez, M. Couzi, A. Tressaud, J. Grannec, J. P. Chaminade, J. L. Soubeyroux, *J. Phys. Condens. Matter* **1990**, *2*, 7373–7386.
[48] J. C. Hancock, K. W. Chapman, G. J. Halder, C. R. Morelock, B. S. Kaplan, L. C. Gallington, A. Bongiorno, C. Han, S. Zhou, A. P. Wilkinson, *Chem. Mater.* **2015**, *27*, 3912–3918.
[49] J.-P. Laval, R. Mayet, *Acta Crystallogr. Sect. C* **2018**, *74*, 229–235.
[50] B. Mehlhorn, R. Hoppe, *Z. Anorg. Allg. Chem.* **1976**, *425*, 180–188.
[51] J.-P. Laval, D. Mercurio Lavaud, B. Gaudreau, *Rev. Chim. Miner.* **1974**, *11*, 742–750.
[52] I. D. Ratnikova, Y. M. Korenev, P. P. Fedorov, B. P. Sobolev, *Zh. Neorg. Khim.* **1997**, *42*, 302–307.
[53] J.-P. Laval, R. Papiernik, B. Frit, *Acta Crystallogr. Sect. B* **1978**, *34*, 1070–1074.
[54] P. P. Fedorov, I. V. Shishkin, I. P. Zibrov, O. V. Pil'gun, B. P. Sobolev, P. I. Fedorov, V. I. Shelyubskij, *Izv. Akad. Nauk SSSR Neorg. Mater.* **1990**, *26*, 1948–1951.
[55] R. Homann, R. Hoppe, *Z. Anorg. Allg. Chem.* **1969**, *368*, 271–278.
[56] R. Hoppe, *J. Inorg. Nucl. Chem.* **1958**, *8*, 437–440.
[57] R. Hoppe, K. Blinne, *Z. Anorg. Allg. Chem.* **1958**, *293*, 251–263.
[58] J. Bandemehr, H. L. Deubner, M. Sachs, F. Kraus, *Z. Anorg. Allg. Chem.* **2018**, *644*, 1721–1726.
[59] O. V. Falaleev, M. L. Afanasiev, É. P. Zeer, *J. Struct. Chem.* **1994**, *35*, 485–491.
[60] V. Wilhelm, R. Hoppe, *Z. Anorg. Allg. Chem.* **1974**, *407*, 13–22.
[61] R. D. Shannon, *Acta Crystallogr. Sect. A* **1976**, *32*, 751–767.
[62] M. S. Kuklin, L. Maschio, D. Usvyat, F. Kraus, A. J. Karttunen, *Chem. Eur. J.* **2019**, *25*, 11528–11537.
[63] K. Eklund, M. S. Kuklin, F. Kraus, A. J. Karttunen, *ChemPhysChem* **2020**, *21*, 802–808.
[64] H. Bode, G. Teufer, *Z. Anorg. Allg. Chem.* **1956**, *283*, 18–25.
[65] C. D. Flint, *J. Mol. Spectrosc.* **1971**, *37*, 414–422.
[66] L. Helmholz, M. E. Russo, *J. Chem. Phys.* **1973**, *59*, 5455–5470.
[67] K. Nakamoto, *Infrared and Raman Spectra of Inorganic and Coordination Compounds*, Wiley, Hoboken, New Jersey, **2009**.
[68] Y. K. Xu, S. Adachi, *J. Appl. Phys.* **2009**, *105*, 013525.
[69] D. Sekiguchi, J. Nara, S. Adachi, *J. Appl. Phys.* **2013**, *113*, 183516.
[70] Q. Zhou, Y. Zhou, Y. Liu, L. Luo, Z. Wang, J. Peng, J. Yan, M. Wu, *J. Mater. Chem. C* **2015**, *3*, 3055–3059.
[71] Q. Shao, L. Wang, L. Song, Y. Dong, C. Liang, J. He, J. Jiang, *J. Alloys Compd.* **2017**, *695*, 221–226.
[72] *STOE WinXPOW*, STOE & Cie GmbH, Darmstadt, Germany, **2015**.
[73] V. Petříček, M. Dušek, L. Palatinus, *Z. Kristallogr.* **2014**, *229*, 345–352.
[74] *OPUS V7.2*, Bruker Optik GmbH, Ettlingen, Germany, **2012**.
[75] A. R. Oganov, A. O. Lyakhov, M. Valle, *Acc. Chem. Res.* **2011**, *44*, 227–237.
[76] A. O. Lyakhov, A. R. Oganov, H. T. Stokes, Q. Zhu, *Comput. Phys. Commun.* **2013**, *184*, 1172–1182.
[77] C. W. Glass, A. R. Oganov, N. Hansen, *Comput. Phys. Commun.* **2006**, *175*, 713–720.
[78] R. Dovesi, A. Erba, R. Orlando, C. M. Zicovich-Wilson, B. Civalleri, L. Maschio, M. Rérat, S. Casassa, J. Baima, S. Salustro, B. Kirtman, *Wiley Interdiscip. Rev.: Comput. Mol. Sci.* **2018**, e1360.
[79] M. S. Kuklin, A. J. Karttunen, *J. Phys. Chem. C* **2018**, *122*, 24949–24957.
[80] J. P. Perdew, K. Burke, M. Ernzerhof, *Phys. Rev. Lett.* **1996**, *77*, 3865–3868.
[81] C. Adamo, V. Barone, *J. Chem. Phys.* **1999**, *110*, 6158–6170.
[82] F. Weigend, R. Ahlrichs, *Phys. Chem. Chem. Phys.* **2005**, *7*, 3297–3305.
[83] F. Pascale, C. M. Zicovich-Wilson, F. López Gejo, B. Civalleri, R. Orlando, R. Dovesi, *J. Comput. Chem.* **2004**, *25*, 888–897.
[84] C. M. Zicovich-Wilson, F. Pascale, C. Roetti, V. R. Saunders, R. Orlando, R. Dovesi, *J. Comput. Chem.* **2004**, *25*, 1873–1881.

Manuscript received: July 6, 2021
Revised manuscript received: August 30, 2021
Accepted manuscript online: August 30, 2021